

See discussions, stats, and author profiles for this publication at: <https://www.researchgate.net/publication/51540970>

Intermolecular Interactions and Electrostatic Properties of the β -Hydroquinone Apohost: Implications for Supramolecular Chemistry

ARTICLE in THE JOURNAL OF PHYSICAL CHEMISTRY A · AUGUST 2011

Impact Factor: 2.69 · DOI: 10.1021/jp2041789 · Source: PubMed

CITATIONS

5

READS

58

7 AUTHORS, INCLUDING:



Yu-Sheng Chen

University of Chicago

122 PUBLICATIONS 1,473 CITATIONS

[SEE PROFILE](#)



Dylan Jayatilaka

University of Western Australia

26 PUBLICATIONS 1,234 CITATIONS

[SEE PROFILE](#)



George A Koutsantonis

University of Western Australia

158 PUBLICATIONS 2,059 CITATIONS

[SEE PROFILE](#)



Mark A Spackman

University of Western Australia

58 PUBLICATIONS 2,924 CITATIONS

[SEE PROFILE](#)

Intermolecular Interactions and Electrostatic Properties of the β -Hydroquinone Apohost: Implications for Supramolecular Chemistry

Henrik F. Clausen,[†] Yu-Sheng Chen,[‡] Dylan Jayatilaka,[§] Jacob Overgaard,[†] George A. Koutsantonis,[§] Mark A. Spackman,[§] and Bo B. Iversen^{*,†}

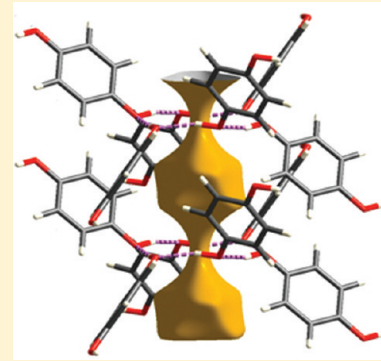
[†]Center for Materials Crystallography, Department of Chemistry and Interdisciplinary Nanoscience Center, Aarhus University, DK-8000 Aarhus C, Denmark

[‡]ChemMatCARS, University of Chicago, Advanced Photon Source, Argonne, Illinois 60439, United States

[§]School of Biomedical, Biomolecular and Chemical Sciences, University of Western Australia, WA 6009, Australia

 Supporting Information

ABSTRACT: The crystal structure of the β -polymorph of hydroquinone (β -HQ), the apohost of a large family of clathrates, is reported with a specific focus on intermolecular interactions and the electrostatic nature of its cavity. Hirshfeld surface analysis reveals subtle close contacts between two interconnecting HQ networks, and the local packing and related close contacts were examined by breakdown of the fingerprint plot. An experimental multipole model containing anisotropic thermal parameters for hydrogen atoms has been successfully refined against 15(2) K single microcrystal synchrotron X-ray diffraction data. The experimental electron density model has been compared with a theoretical electron density calculated with the molecule embedded in its own crystal field. Hirshfeld charges, interaction energies and the electrostatic potential calculated for both models are qualitatively in good agreement, but small differences in the electrostatic potential persist due to charge transfer from all hydrogen atoms to the oxygen atoms in the theoretical model. The electrostatic potential in the center of the cavity is positive, very shallow and highly symmetric, suggesting that the inclusion of polar molecules in the void will involve a balance between opposing effects. The electric field is by symmetry zero in the center of the cavity, increasing to a value of $0.0185 \text{ e}/\text{\AA}^2$ ($0.27 \text{ V}/\text{\AA}$) 1 \AA along the 3-fold axis and $0.0105 \text{ e}/\text{\AA}^2$ ($0.15 \text{ V}/\text{\AA}$) 1 \AA along the perpendicular direction. While these values are substantial in a macroscopic context, they are quite small for a molecular cavity and are not expected to strongly polarize a guest molecule.



INTRODUCTION

Understanding of supramolecular chemistry supports the design and development of materials for a vast number of potential applications (sensors, nonlinear optics, switches, etc.).^{1,2} Yet, it is striking that the fundamental chemical interactions governing simple self-assembly processes are not well understood.^{3,4} Atomic level information is necessary for understanding self-assembly at a fundamental level, and molecular crystals are the ideal supramolecular entities for obtaining such information. A significant challenge in studying molecular crystals is the inherent complexity, as a typical molecular crystal will have numerous superimposed intermolecular interactions, all of which contribute to the cohesive energy of the solid. Detailed understanding of intermolecular interactions presently relies predominantly on the tabulation of interatomic distances and geometries, which for complex systems becomes very difficult to interpret. In the past decade the much more easily interpretable approach of Hirshfeld surface analysis has been introduced by Spackman and co-workers, and this promises to significantly improve our understanding of intermolecular interactions.^{5,6}

Assembly of porous host–guest structures from organic molecules has been known for a very long time. HQ has the ability

of encaging a variety of small molecules, such as CO_2 , CH_3OH , and CH_3CN ,^{8–11} and it is, therefore, a well-suited system for studies of supramolecular intermolecular interactions. HQ itself exists in three polymorphs under ambient conditions (α -, β -, and γ -forms), where the metastable β -modification, denoted 1, forms relatively rigid spherical cages with nearly 5 \AA free diameter, see Figure 1. The cavity is formed by six benzene rings on the side and two six-membered rings of hydrogen bonded hydroxyl groups on the top and bottom. Clathrates of HQ have the general formula $3\text{C}_6\text{H}_4(\text{OH})_2 \cdot xS$, where S is the solvent guest molecule or atom, and x ranges from 0 to 1. Unlike many other clathrate host systems, crystals of β -HQ can also be prepared without any enclathrated solvent, and this serves as a reference system for investigating the interactions between host and guest molecules in the clathrates.^{12,13} Caspari, reported in 1927, the β -quinol structure, $\text{C}_6\text{H}_4(\text{OH})_2$,¹⁴ although it would appear that

Special Issue: Richard F. W. Bader Festschrift

Received: May 5, 2011

Revised: July 6, 2011

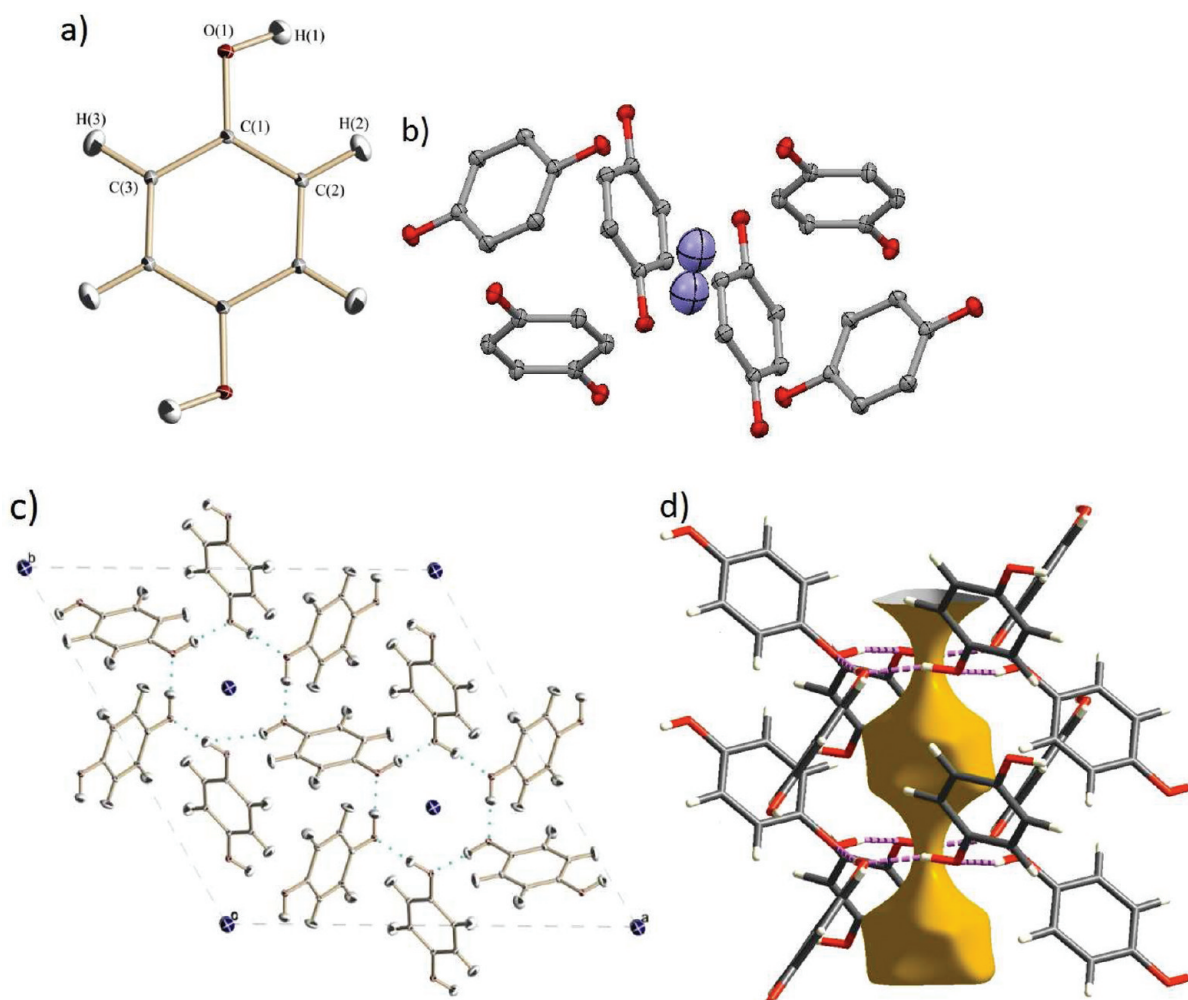


Figure 1. (a) Individual HQ unit with atomic labeling. (b) Cavity generated by six HQ molecules including a small residue of atmospheric air. (c) Packing diagram illustrating the hydrogen-bonded hexagons viewed along the *c*-axis of the unit cell of **1**. (d) Void generated by six HQ molecules, represented by the 0.0003 a.u. isosurface of the procrystal electron density.⁷ Thermal ellipsoids are drawn at a 90% level.

the structure reported in that work was actually that of the methanol clathrate.

Determination of the charge density (CD) of these systems can provide estimates of the electrostatic nature of the host lattice, as well as the guest molecules, and therefore provide detailed quantitative information about the intermolecular interactions. In the present study we use very low temperature single crystal synchrotron X-ray diffraction CD analysis of the “empty” β -form of HQ to establish the electrostatic properties of the apohost, especially the potential inside the unfilled cavity. This provides a reference for our future studies of actual host–guest systems and also provides experimental evidence to confirm the predictions made on basis of the empirical calculations that “the distribution of charges around the cage favors the positively charged atoms of the molecule to be located in the center of the cavity”.¹⁵

■ EXPERIMENTAL SECTION

Synthesis. Synthesis of the empty clathrate of the β -hydroquinone proved rather difficult, as the solvent reported by Lindeman et al. did not produce the anticipated crystals.¹² Evaporation of a solvent larger than the cavity of β -HQ proved

to be successful, but phase pure samples have not been obtained to date. For **1**, $C_6H_4(OH)_2$, hydroquinone (0.550 g), and water-free propan-2-ol (10 mL) was mixed in a glass beaker, and the solvent was slowly evaporated at room temperature. Colorless transparent crystals were obtained, but examination of the sample revealed that it consisted of a mixture of three phases. Besides sample **1**, the α -form of hydroquinone and a cocrystal of hydroquinone and isopropanol were also obtained.^{16,17}

Synchrotron X-ray Diffraction Experiments. The crystals of **1** were taken to the Advanced Photon Source in Chicago for single crystal X-ray diffraction experiments. A crystal of **1** was mounted on a Bruker D8 diffractometer, equipped with an APEXII CCD detector, at the ChemMatCARS beamline (ID-15). Several crystals were tested before a suitable minute specimen of **1** was found ($0.02 \times 0.02 \times 0.02$ mm³), as the crystal system has a tendency toward merohedral twinning. The present study was only feasible due to the immense intensity of the third generation synchrotron at the Advanced Photon Source, and indeed multipole refinement of data measured at 100(1) K on a laboratory source was unsuccessful. The synchrotron data were collected using a wavelength of 0.413 Å (30 KeV) obtained from a diamond (111) monochromator, and the crystal was cooled to

15(2) K using an open flow Helium cryostream. The use of high energy X-rays and a small crystal provides data in which systematic errors such as absorption and extinction are very significantly reduced. The data collection was performed in φ -scan mode using steps of 0.3° at two different ω -angles and with a fixed χ -angle. Three different 2θ settings (-30 , -25 , and -10) of the detector at a distance of 5 cm were used yielding a maximum resolution in $\sin \theta/\lambda$ of 1.18 \AA^{-1} . A total of 40725 reflections were collected and integrated with SAINT+.¹⁸ Subsequently, these were corrected for oblique incidence due to imperfect absorption of the X-ray signal on the CCD phosphor,¹⁹ using the program SADABS with a detector phosphor efficiency fixed at 0.604.²⁰ This program also corrects for slight misalignment of the crystal with the φ -axis, absorption and other systematic effects. Outlier rejection and data averaging yielded 3844 unique reflections with an internal agreement factor, R_{int} , of 3.37% using the program SORTAV.²¹ Only reflections measured three times or more were used in the subsequent refinements to limit the number of spurious outliers. Selected experimental details are given in Table 1.

Powder X-ray Diffraction. The *as synthesized* sample was examined using powder X-ray diffraction data measured on a Siemens D-5000 diffractometer, using Cu K α radiation ($\lambda = 1.54 \text{ \AA}$), and Figure 2 shows a close-up of the low-order region. The full powder pattern is included in the Supporting Information.

The crystals obtained were a mixture of the cocrystal of **1**, the α -form of hydroquinone and a cocrystal of hydroquinone and isopropanol.^{16,17} The sample was re-examined after 14 days where the diffraction pattern revealed significant changes, Figure 2. The β -HQ phase is no longer visible after 14 days, and hence, it is metastable in the isopropanol solution and will, over a period of time, convert into the α -HQ phase, which is the thermodynamically stable phase of HQ.²²

Multipole Refinement of **1.** The structure of **1** was obtained using the direct methods program SHELXS, and it was subsequently refined using the independent atom model in SHELXL.¹⁸ In the refinement of the structure symmetry, related residual peaks were observed in the cavity of **1** at a distance of 1.10 \AA , which match the bond length in a nitrogen molecule.²³ The occupancy of the N₂ molecule was refined and found to be approximately 6% in each cavity. Gibson et al. has reported the β -HQ structure with 50% inclusion of nitrogen,²⁴ where a tilt of 11° of the N₂ molecule at low temperatures was observed. This could not be refined in the present study due to the low occupancy. In combination with the latter, the residual density at the inversion points leads to an enlargement of the ADPs of N₂, which possibly also results in an overestimation of the occupancy in the IAM refinement. Even though the model was refined as nitrogen, it is likely that both oxygen and nitrogen from the atmosphere has been captured within the structure. The model obtained from SHELXL (atomic positions, atomic displacement parameters (ADPs) and N₂ occupancy) was chosen as a starting point for the multipole refinement in program XD.²⁵ The model was refined against the high order data, $\sin(\theta)/\lambda > 0.8 \text{ \AA}^{-1}$, to obtain less biased atomic positions and ADPs for the heavy atoms. The InvariomTool program and database were used to implement a starting model with aspherical invarioms.^{26,27} Isotropic ADPs of hydrogen are commonly used in charge density modeling, but like the heavier atoms hydrogen also vibrates anisotropically. The SHADE server (Simple Hydrogen Anisotropic Displacement Estimator) enables one to estimate anisotropic hydrogen motion from the vibration of the

Table 1. Crystallographic and Experimental Details of the Single Crystal Synchrotron X-ray Diffraction Experiment on **1**

empirical formula	C ₆ H ₄ (OH) ₂ ·0.02N ₂
formula weight (g/mol)	110.58
space group	$R\bar{3}$
Z	9
T (K)	15(2)
λ (Å)	0.41328
a, c (Å)	16.5249(3), 5.3430(1)
V (Å ³)	1263.55(4)
ρ_{calc} (g/cm ³)	1.302
μ_1 (mm ⁻¹)	0.0101
$T_{\text{max}}/T_{\text{min}}$	0.903/1.000
N _{measured}	40725
N _{unique} , N _{unique} (nmeas ≥ 3)	3844, 2909
R _{int}	0.0337
$\sin(\theta_{\text{max}})/\lambda$ (Å ⁻¹)	1.18
N _{par} , N _{obs} ($I > 2\sigma(I)$)	127, 2256
R _{2o} (F), R _{2o} (F ²)	0.0148, 0.0184
R _{all} (F), R _{all} (F ²)	0.0226, 0.0202
R _w (F), R _w (F ²)	0.0163, 0.0325
GoF	0.4706

heavier atoms,²⁸ and a Hansen-Coppens multipole model was subsequently refined using anisotropic hydrogen ADPs.²⁹ Gradually the complexity of the model was increased, ending in corefinement of all structural and electronic parameters of the framework structure. The small nitrogen residue was described as spherical atoms due to the low occupancy, which was kept fixed at the value obtained in the IAM refinement. The residual at the inversion point caused unrealistic shortening of the bond and, hence, the position of the unique atom was fixed. The enclathrated molecular residue is not strongly interacting with the host-framework, which precludes significant charge transfer. The noncrystallographic mirror plane of the aromatic carbon atoms was partially observed in the final model, as quadrupoles and higher multipoles contributing to the asymmetry were found to be negligible. The final model included all symmetry-allowed multipoles up to hexadecapole level on the non-H atoms, with the exception of the negligible poles due to mirror symmetry, which were not refined for the carbon atoms. The aromatic hydrogen atoms were refined using a monopole, a bond-directed dipole, and a quadrupole, whereas the more strongly bonded hydroxyl hydrogen atom was modeled with a monopole, all dipoles, and a bond-directed quadrupole. Hydrogen atomic positions were after each refinement cycle reset to give bond distances equal to standard average neutron diffraction values.³⁰ Two radial expansion–contraction parameters were added for both carbon and oxygen, whereas one was added to describe the hydrogen atoms as this improved the model significantly. Further expansions of the model were tested including additional κ parameters, anharmonic vibrational parameters, and an extinction parameter, but the residual density maps and agreement factors did not improve, and the extra parameters were discarded. The refinement details are listed in Table 1.

The final model included 127 parameters which were refined against 2256 observations ($I > 2\sigma(I)$). The Hirshfeld rigid bond test was satisfactory fulfilled with a mean value of the difference of mean square displacement amplitudes (DMSDA) being

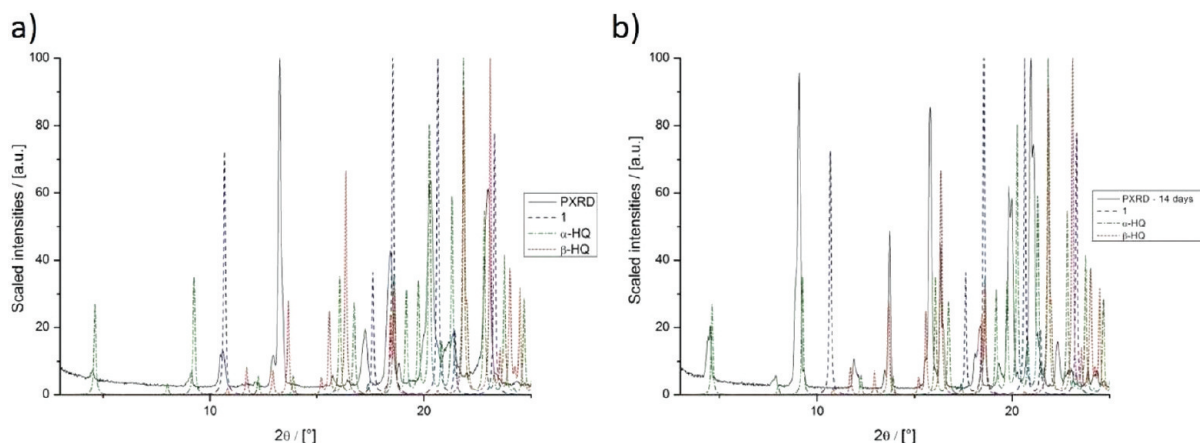


Figure 2. Powder X-ray diffraction patterns (black) of (a) the as-synthesized sample and (b) the sample after 14 days in isopropanol. Theoretical patterns obtained from experimentally determined single crystal structures at 100 K of **1** (blue), α -hydroquinone (green) and the cocrystal of hydroquinone and isopropanol (red) are shown for comparison.

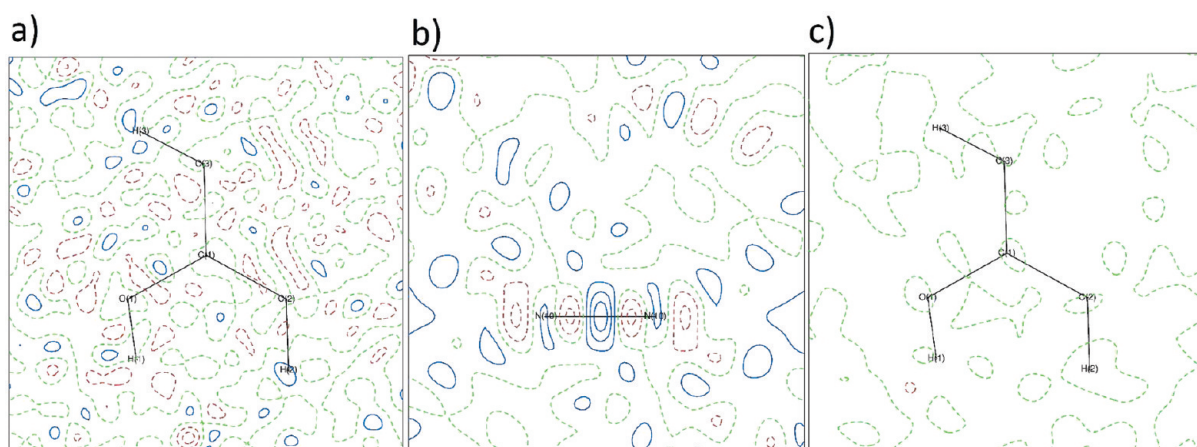


Figure 3. Residual maps of **1** obtained using all data of (a) the hydroquinone molecule and (b) the molecular residue. In (c) a residual density map of the hydroquinone molecule obtained using data below 0.8 \AA^{-1} is shown. The contour intervals are 0.05 e\AA^{-3} with solid blue contours being positive, red dashed negative, and green the zero contour.

$\Delta_{A-B} = 1.33 \text{ pm}^2$ (the maximum value was 2 pm^2),^{31,32} see Supporting Information. A Fourier peak search of the residual density resulted in peaks ranging from 0.17 to -0.12 e/\AA^3 , with the strongest peak located at the high symmetry inversion point on the 3-fold inversion axis, which coincides with the bond center in the small molecular residue. The remaining 10 strongest peaks and holes are located more than 0.7 \AA from any atom. Inspection of the residual density maps showed that the residual density is more pronounced near the molecular residue at the high symmetry 3-fold inversion point, Figure 3.

Previously the effect on refinement residuals of removing outlier reflections based on the deviation from the model has been studied,³³ where it was established that the refined multipole model was not affected by “cleaning” the data for severe outliers, as these typically are very weak high-angle reflections. The cleaned data set, therefore, actually creates a more reliable view of the errors in the experimental multipole model and, hence, increases the ability to identify model flaws. Figure 3 also shows the residual density maps obtained using the data below 0.8 \AA^{-1} , that is, the data carrying the majority of the CD information.

Further residual maps have been deposited in Supporting Information. The observed residuals are very small, and appear to be featureless in the plane of the hydroquinone molecules with extremes less than 0.05 e\AA^{-3} . Analysis of the residual density using jnk2RDA³⁴ reveals a small shoulder due to a residual near the molecular residue, see Supporting Information. Noise has a tendency to concentrate at high symmetry points and axes,³⁵ and this accidentally coincides with the position of the small molecular residue.

Quantum Mechanical Calculations. Quantum mechanical calculations on β -HQ were carried out at the BLYP/cc-pVTZ level using the program Tonto.^{36,37} In this calculation, charges were introduced around the central isolated HQ molecule to simulate the effect of the crystal environment. Atomic charges and dipoles were obtained from atoms defined by Hirshfeld (stockholder) partitioning using spherically averaged atomic electron densities calculated for the atoms in their spin ground states.³⁸ The numerical integrations used a Lebedev grid³⁹ and 35 radial points for H and 40 for the remaining atoms, according to the formula of Mura and Knowles.⁴⁰ These charges and dipoles (simulated by two opposite point charges separated by a distance

Table 2. Topological Analysis of the Chemical Bonding in **1^a**

bond	R (Å)	R _{ij} (Å)	d ₁ (Å)	ρ (eÅ ⁻³)	∇ ² ρ (eÅ ⁻⁵)	ε	G (hartree Å ⁻³)	V (hartree Å ⁻³)	H (hartree Å ⁻³)
O(1)–C(1)	1.3734(3)	1.3734	0.8262	1.98	-18.9	0.10	1.6	-4.6	-3.0
O(1)–H(1)	0.9670(2)	0.9674	0.7784	2.29	-55.2	0.03	0.6	-5.1	-4.5
C(1)–C(2)	1.3937(3)	1.3939	0.7290	2.13	-18.9	0.25	1.9	-5.2	-3.3
C(1)–C(3)	1.3910(3)	1.3910	0.7130	2.14	-19.9	0.25	1.9	-5.3	-3.3
C(2)–C(3)	1.3920(3)	1.3920	0.7009	2.09	-17.5	0.17	1.9	-5.1	-3.2
C(2)–H(2)	1.0830(2)	1.0830	0.7033	1.92	-22.2	0.02	1.4	-4.3	-2.9
C(3)–H(3)	1.0830(2)	1.0830	0.6851	1.94	-23.5	0.01	1.3	-4.3	-3.0
O(1)…H(1)	1.6899(2)	1.6916	1.1217	0.34	2.2	0.03	0.2	-0.3	-0.1

^a R is the bond distance between the two atoms. R_{ij} (Å) is the sum of the distance from the first atom through the BCP to the other atom. d₁ (Å) is the distance from the atom to the BCP. ρ is the electron density (e/Å³), ∇²ρ the Laplacian (e/Å⁵), and ε the ellipticity of the bond. G, V, and H are the local kinetic, potential, and total energy densities estimated using the Abramov functional (in a.u.).⁴⁵ The random errors of ρ and ∇²ρ estimated from the least squares refinement are significantly smaller than systematic errors between slightly different models. Correspondingly values of ρ are presented with two decimals, while the Laplacian values are truncated after the first decimal.

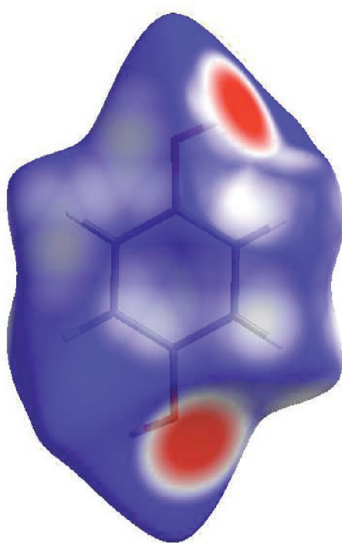


Figure 4. Hirshfeld surface of the HQ molecule in **1** with d_{norm} mapped ranging from -0.5 (blue) to 0.5 Å (red).

of 0.001 a.u.) were placed on the atomic positions of the surrounding molecules within 8 Å from the central HQ molecule. The charges and dipoles of the Hirshfeld atoms were calculated self-consistently from the molecule embedded in its own field. The quantum mechanical calculation was repeated in the presence of these cluster charges, and subsequently, the Hirshfeld (stockholder) charges were recalculated and propagated to the cluster. This sequential propagation of charges was performed three times, which resulted in the change of the Hirshfeld charges being negligible (<0.0001 e). It should be noted that the enclathrated N₂ residue was not included in the quantum mechanical calculations of the β-HQ structure.

RESULTS AND DISCUSSION

Structure of **1.** The structure of β-HQ reported by Lindeman et al.¹² is ostensibly that of the apohost, where the voids are unoccupied. In the structure presented here, there is approximately 6% occupancy of atmospheric air enclathrated in the cavity. The host structure consists of HQ molecules, which generate hydrogen bonded hexagons of hydroxyl groups to form

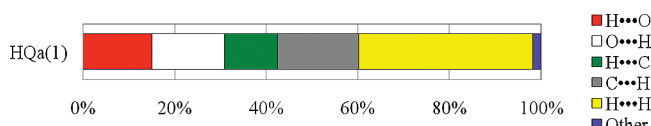


Figure 5. Close contacts on the Hirshfeld surfaces of the HQ molecule in **1** broken down into six different basic interaction types: O–H···O hydrogen bonding, both donor (red) and acceptor (white); H···C contacts (green); C···H contacts (gray); H···H contacts (yellow); and all other contacts (blue). The notation C···H refers to close contacts between C atoms inside the Hirshfeld surface (i.e., belonging to the HQ molecule) and H atoms outside the surface (i.e., belonging to other HQ molecules).

a rhombohedral HQ framework with cavities, see Figure 1. The framework consists of two interconnecting hydrogen-bonded networks which only have weak interactions between them. The structure of **1** contains one unique HQ molecule and a total of 9 molecules in the unit cell, which creates three cavities per unit cell. The ratio between hydroquinone molecules and possible enclathrated solvent molecules is, hence, 3:1.

The aromatic ring appears to be fully delocalized and bond lengths are given in Table 2. The corresponding angles are O(1)–C(1)–C(2) 122.12(2)°, O(1)–C(1)–C(3) 117.52(2)°, C(1)–C(2)–C(3) 119.48(2)°, C(2)–C(1)–C(3) 120.36(2)°, and C(1)–C(3)–C(2) 120.16(2)°. The angle between the aromatic system and the hydroxyl oxygen atom of **1** deviates by ~2.5° from 120° to accommodate the hydrogen atom in the plane of the aromatic ring. The hydroxyl groups of the HQ molecule in the structure of **1** are both donors and acceptors of hydrogen bonds. There are no strong interactions expected between the host and guest, and hence even though a small molecular residue is present, the structure will be used as a model compound for the host network for HQ clathrates.

Hirshfeld Surface of **1.** The Hirshfeld surface of the HQ molecule in the β-HQ has been generated (N₂ was excluded due to the low occupancy) and the normalized contact distance, d_{norm}, plotted using the CrystalExplorer program, Figure 4.^{9,10,41}

The closest contacts on the Hirshfeld surface are not unexpectedly observed for the O···H and H···O hydrogen bonding interactions (red regions in Figure 4). The structural packing of **1** cannot be described adequately in three dimensions only by the use of the hydrogen bonding pattern, because the structure consists of two interconnected hydrogen-bonded networks.

Even though hydrogen bonding is anticipated to be the strongest interaction between the HQ molecules, the remaining close contacts cannot be neglected, Figure 5. These contacts cover around 69% of the Hirshfeld surface, and include a large proportion of nondirectional H···H contacts (~38%). The intermolecular contacts can be depicted in a fingerprint plot, Figure 6, where d_i is the closest internal distance from a given point on the Hirshfeld surface and d_e is the closest external contact. For the H···H contacts d_i and d_e stretch far in the fingerprint plot due to the empty cavity of the structure. The C···H (label "5") and H···C (label "4") close contacts exhibit the characteristic "wings", indicating that there are significant directional C–H···π interactions. These are the weak interactions between the two interpenetrating hydrogen-bonded nets-

works. The short hydrogen and oxygen donor and acceptor features are labeled "3" and "1" in Figure 6. The C–H···π interaction between HQ molecules is clearly visible in the fingerprint plot obtained from the distribution of close contacts, which demonstrates that diverse interactions can easily be detected using the normalized contact distance obtained from Hirshfeld surface partitioning. The volume inside the HQ Hirshfeld surface was determined to be 135.1 \AA^3 , which due to the empty cavity is $\sim 10 \text{ \AA}^3$ larger than a series of HQ molecules in three cocrystals reported by Clausen et al.¹⁶

Charge Density of 1. Static deformation densities and Laplacian distributions in the plane of the HQ molecule as obtained from the multipole model are shown in Figure 7. The bonding regions of the aromatic system in both the static deformation density and Laplacian distribution show single peak maxima. Furthermore, the deformation density is negative near the oxygen nucleus, which is expected from theory.⁴² These two deformation density features are typical quality marks for an experimental multipole density.⁴³ Together with the very low residual density presented in Figure 3, these quality features suggest that the present experimental CD of 1 is of high quality, and thus, reliable properties of the β-HQ can be derived.

In Figure 8, the theoretical deformation density and Laplacian distributions are shown. Although the features are qualitatively the same as obtained from experiment, the density observed in the bonding regions of the theoretical model is slightly higher than in the experimental model.

Chemical bonding can be characterized using topological analysis of the electron density within the framework of the quantum theory of atoms in molecules (QTAIM).⁴⁴ In the QTAIM atoms that are bonded together are connected by a bond path, and the bond critical point (BCP) is located at the minimum along this path. The BCP properties of the intramolecular bonds of the HQ molecule in 1 obtained from the experimental multipole model are summarized in Table 2.

The electron density for the intramolecular bonds falls in the range from 1.9 to $2.3 \text{ e}/\text{\AA}^3$, and these bonds can be further divided into subgroups depending on their bond character,

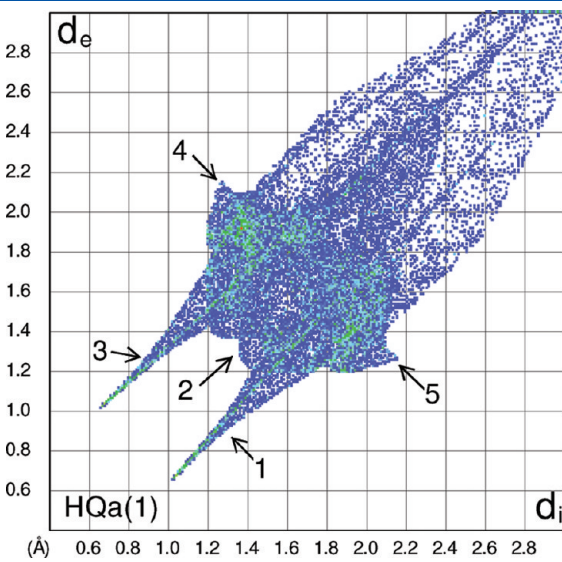


Figure 6. Fingerprint plot of the HQ molecule in 1. Close contacts are divided into five regions; 1 is O···H, 2 is H···H, 3 is H···O, 4 is H···C, and 5 is C···H.

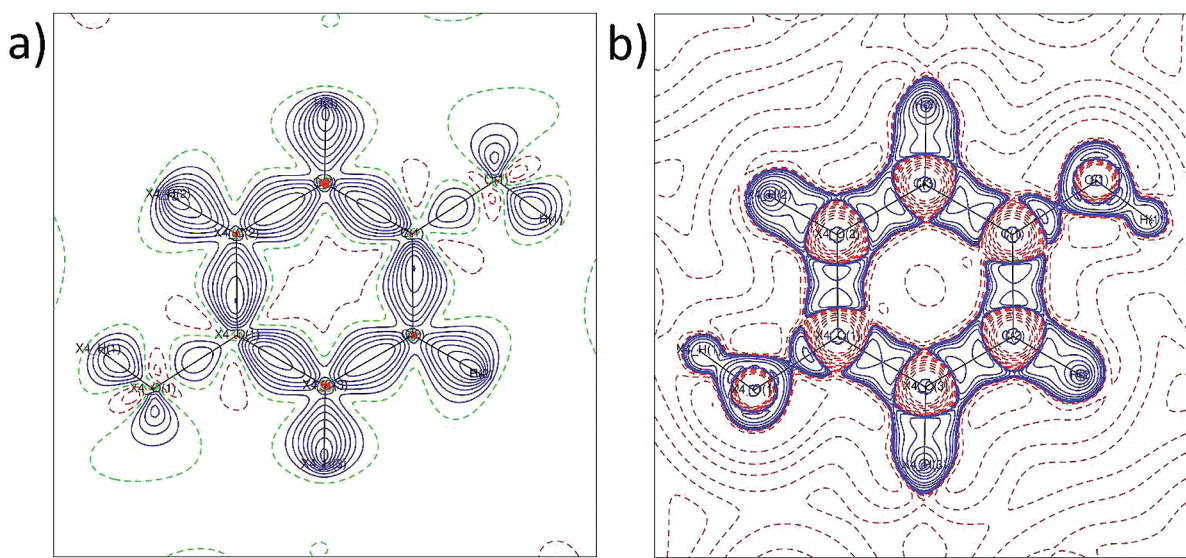


Figure 7. Experimental static deformation density (a) and Laplacian distribution (b) of the HQ molecule. For the deformation density, the contour interval is $0.1 \text{ e}/\text{\AA}^3$ with solid contours positive and dashed negative. For the Laplacian map, the contour level is $2^x \cdot 10^y \text{ e}/\text{\AA}^5$ ($x = 1-3$ and $y = -2, -1, 0, 1, 2$) with dashed lines positive and solid lines negative.

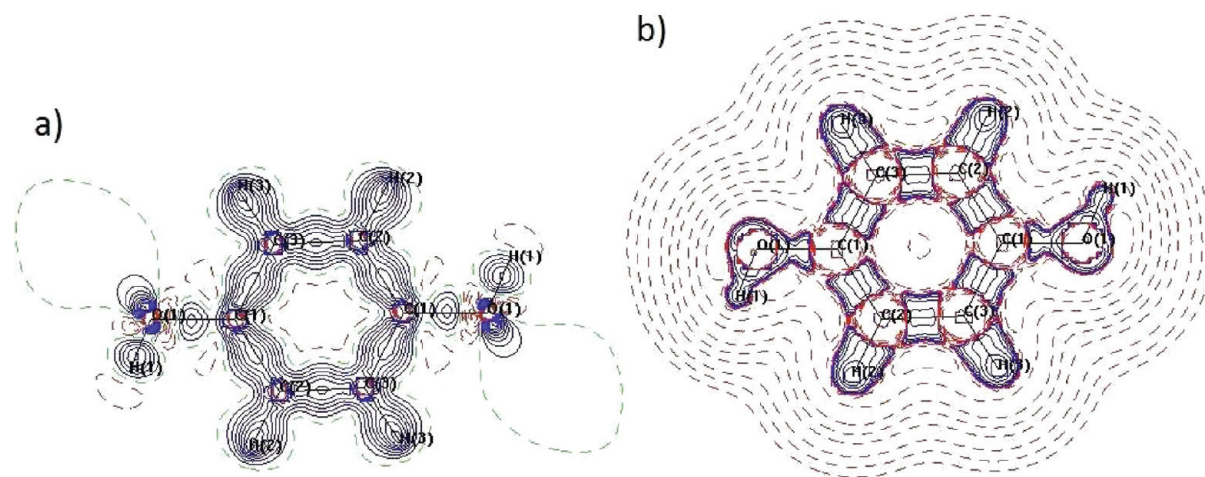


Figure 8. Static deformation density (a) and the Laplacian distribution (b) of the HQ molecule from the quantum mechanical calculation using TONTO. Contours as in Figure 7.

Table 3. Atomic Properties of the Apohost Structure, 1^a

	experimental model						TONTO	
	monopole charge (e)	Bader charge (e)	Hirshfeld charge (e)	TBV (Å ³)	ΔTBV (Å ³)	dipole (Bader; a.u.)	Hirshfeld charge (e)	dipole (Hirshfeld; a.u.)
O(1)	-0.02	-1.02	-0.12	15.9	8.5	0.20	-0.22	0.27
C(1)	0.02	0.39	0.06	9.1	2.3	0.62	0.04	0.11
C(2)	0.05	-0.02	-0.07	11.8	4.4	0.21	-0.06	0.05
C(3)	0.12	0.01	-0.06	11.1	0.8	0.15	-0.06	0.04
H(1)	0.07	0.64	0.16	1.4	0.1	0.11	0.20	0.24
H(2)	-0.11	0.00	0.01	7.3	5.5	0.15	0.06	0.15
H(3)	-0.13	0.01	0.02	6.7	1.3	0.16	0.04	0.14
Total	0.00	0.00	0.00	63.3			0.00	

^a Atomic charges are estimated from the monopole population (Monopole), the zero-flux surface condition (Bader), and the Hirshfeld (stockholder) partitioning. TBV is the total basin volume (zero flux condition) and ΔTBV is the volume difference between TBV and the volume with electron density above 0.002 a.u. in the units of Å³. The size of the dipole moment is defined as the length of the dipole vector. Hirshfeld charges and Hirshfeld dipole moments are listed from the theoretical calculations (TONTO).

namely single or aromatic. The density at the BCPs of the aromatic bonds range from 2.09 to 2.14 e/Å³, whereas the single bonds in general have values in the range from 1.92 to 1.98 e/Å³, with one exception, the O–H bonds of the hydroquinone molecules where the density is higher, 2.29 e/Å³. The Laplacian at the BCP is negative for all intramolecular bonds, which is expected for covalently interacting atoms. The Abramov functional can be used to estimate the local kinetic, potential, and total energy densities, Table 2, and these also indicate that the intramolecular bonds are of a covalent nature. The ellipticities of the single bonds are in general lower than for the aromatic bonds due to the more symmetric electron density distribution around the single bond. However, it is noteworthy that the C–O bond has a higher ellipticity relative to the other single bonds, which presumably is due to the conjugation of the oxygen lone pair with the aromatic system. The intermolecular hydrogen bonds of the HQ molecules are primarily closed shell type interactions with positive Laplacian values. However, the negative local kinetic energy density reveals that there are some covalent contributions present in these hydrogen bonds. The energy of the hydrogen bond can be crudely estimated using the approximation of Espinosa et al.,⁴⁶ which results in $E(\text{HB}) = 1/2V = -62 \text{ kJ/mol}$.

The zero flux condition divides molecules into discrete non-overlapping atomic basins from which properties of the separate atoms can be derived. One particularly attractive feature of this partitioning is that the atomic properties such as energy, volume, or charge are additive.⁴⁴ The atomic properties obtained for the host-structure 1 using the zero-flux condition and subsequent integration of the atomic basins are listed in Table 3 along with the experimental atomic charges obtained using the Hirshfeld (stockholder) partitioning.³⁸

The summation of the topological charges of the Bader atoms, as well as the Hirshfeld atoms, of the host structure results in an overall neutral network, which is in correspondence with an overall neutral crystal. As expected, there are clear differences between the Bader charges determined from the quantum mechanical zero flux condition and the fuzzy boundary Hirshfeld charges. The latter values are quite close to zero since they are obtained from division of the deformation density among the atoms, whereas the discrete Bader charges have much higher values. The Bader charges more clearly reflect the expected chemistry of the molecule, with the oxygen being negative and the hydroxide hydrogen atom H(1) more positive than the hydrogen atoms bonded to carbon. The strong polarization

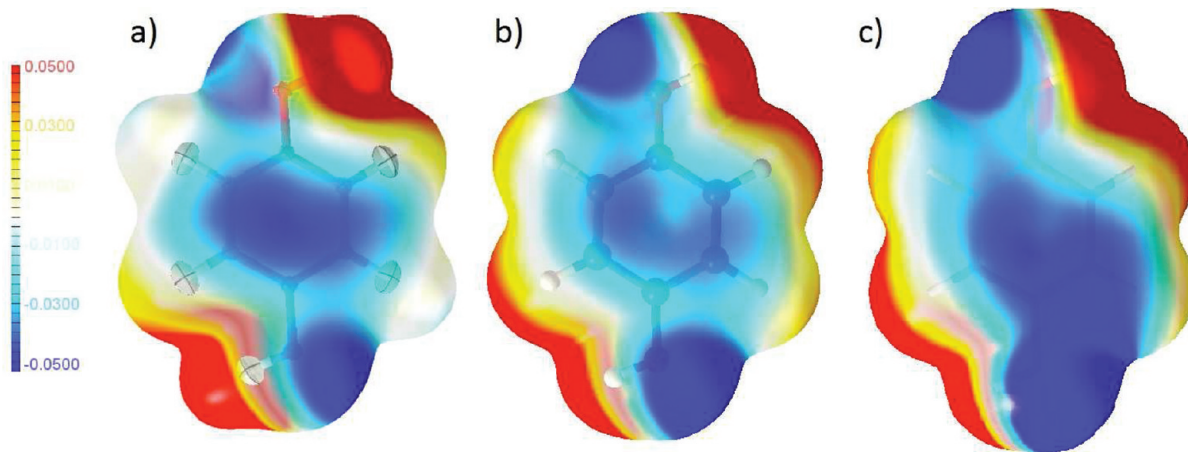


Figure 9. The electrostatic potential calculated from (a) the multipole model, (b) theory on an isolated molecule, and (c) theory on a molecule embedded in a crystal field. The electrostatic potentials were visualized using MoleCoolQt.⁴⁹ The electrostatic potential is plotted on the electron density isosurface of $0.01 \text{ e}/\text{\AA}^3$, with values ranging from -0.05 (blue) to $0.05 \text{ e}/\text{\AA}$ (red).

around the oxygen atom is reflected in the C(1) atomic dipole moment being larger than for C(2) and C(3). In the Hirshfeld partitioning of the deformation density, an atom is assigned the same fraction of the charge in a given point as it has in the promolecule, and this scheme, for example, does not account for the electronegativities of the atoms. Correspondingly, the values are quite close to zero. However, when comparing the Hirshfeld charges derived separately from experiment and theory, they are quite similar, although small distinct differences are apparent. The charges of the hydrogen atoms are all less positive in the experimental model, whereas the oxygen atom is less negative. It should be stressed that the dipole moment values are not directly comparable between theory and experiment, as the theoretical values are obtained from the Hirshfeld definition of the atom and the experimental values from the quantum mechanical zero flux condition. The total volume of the atomic basins comprising the HQ molecule determined from the zero flux surface is 126.6 \AA^3 , which is $\sim 10 \text{ \AA}^3$ less than the obtained Hirshfeld volume. This variation of volume is due to the empty cavity in the HS calculation as the molecular residue was excluded from the calculation.

Electrostatics of 1. The total interaction energy between a molecule and its surroundings is constituted of different terms, and we have estimated the largest term, the electrostatic energy, from the charge density. The electrostatic interaction energy was calculated for the inclusion of a hydroquinone molecule into a cluster consisting of all molecules within an intermolecular radius of 3.5 \AA . This mimics the crystal environment using the 10 nearest molecules. The two strongest individual electrostatic interactions are $\text{C}-\text{H}\cdots\pi$ and $\text{O}-\text{H}\cdots\text{O}$, and from the multipole model their energies are estimated to be -6 and -88 kJ/mol , respectively. The experimentally determined electrostatic interaction energy of the HQ molecule with the entire cluster is -378 kJ/mol . From the theoretical calculations the electrostatic interaction energy can be estimated as the difference between the polarized isolated molecule in an optimized geometry and the polarized molecule in the crystal cluster, and this gives a value of -477 kJ/mol . Comparison with the experimental value shows that theory gives a higher electrostatic interaction energy, which was to be expected due to the more prominent bonding features and larger charge difference between oxygen and hydroxyl hydrogen in the theoretical model.

The electron density and the overall charge state of the structure are important, as inclusion properties of the host-structure will depend strongly on the CD. The charge of the framework will influence the electrostatic terms, which contributes to the interaction energy between molecular fragments. Theoretical modeling of hydrogen storage in metal organic frameworks (MOF) has revealed that the host–guest interactions are promoted by the local polarity of the host which induces a dipole in the H_2 guest molecule, and therefore the electrostatic surface of the host is great importance.⁴⁷ Similarly it has been shown that slight changes in the three-dimensional linkage between Mn atoms in MOFs can lead to a reversal of the polarity of benzene dicarboxylic acid linker molecules, which leads to a completely different electrostatic potential in the MOF cavity.⁴⁸

For 1 the electrostatic potential (EP) has been calculated from the multipole model and it is plotted on an electron density isosurface in Figure 9. Electrostatic potentials were also calculated from theoretical calculations of an isolated molecule and a molecule embedded in the crystal field. The theoretical electrostatic potential overall is similar to the experimental result. However, the differences of the charge distributions can be recognized in the more electronegative region at the oxygen atoms and more electropositive region at the aromatic hydrogen atoms in the theoretical model. The theoretical model enhances the local polarity compared with the experimental model, which leads to higher electrostatic interaction energies with potential guest molecules. The difference observed in the electrostatic potential between theory and experiment is in agreement with the distribution of charges observed using the Hirshfeld partitioning as well as the calculated interaction energies.

From the electrostatic potential mapped on the electron density isosurface it is difficult to assess if “the distribution of charges around the cage favors the positively charged atoms of the molecule to be located in the center of the cavity”.¹⁵ On the other hand, mapping of the electrostatic potential along the cavity 3-fold inversion axis reveals that the center of the cavity is close to zero potential, Figure 10. The electrostatic potential increases when moving along the 3-fold inversion axis of the unit cell away from the center of the cavity. The electric field in the cavity shows similar features, as is due to inversion symmetry being zero at the center of the cavity, but moving along the 3-fold

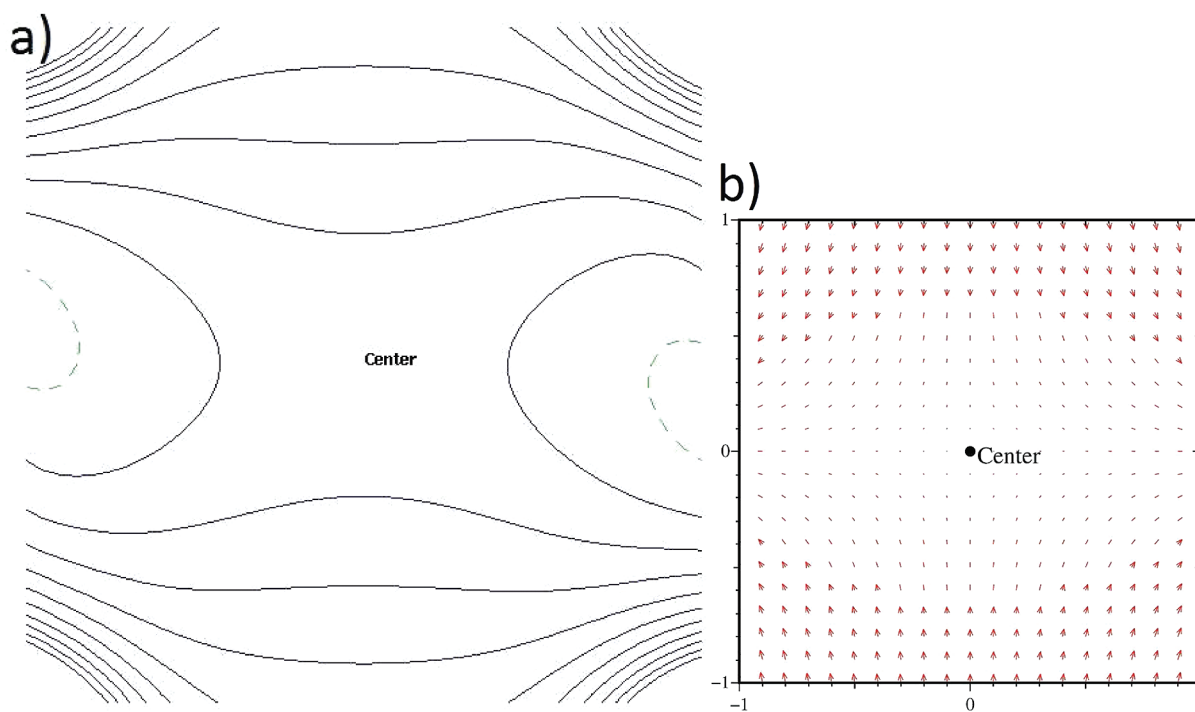


Figure 10. (a) Electrostatic potential of the cavity plotted in a $4 \times 4 \text{ \AA}^2$ plane parallel to the *a*- and *c*-axes of the unit cell and through the center of the cavity. The contour level is 0.01 e \AA^{-1} with blue being positive and green the zero contour. (b) Electric field plotted in a $2 \times 2 \text{ \AA}^2$ plane at the center of the cavity.

inversion axis, the field increases and points toward the center. Overall, this generates a three-dimensional saddle point in the EP located at the center of the cavity with the minimum along the 3-fold inversion axis. The electric field is zero in the center of the cavity, and increases to a value of $0.0185 \text{ e}/\text{\AA}^2$ ($0.27 \text{ V}/\text{\AA}$) 1 \AA along the 3-fold axis and $0.0105 \text{ e}/\text{\AA}^2$ ($0.15 \text{ V}/\text{\AA}$) 1 \AA along the perpendicular direction. While these values are substantial in a macroscopic context, they are quite small for a molecular cavity and not expected to strongly polarize a guest molecule.

Overgaard et al. reported a funnel-shaped EP in a chromium-wheel host complex $[\text{Cr}_8\text{F}_8(\text{tBuCO}_2)_{16}]$ with a three-dimensional saddle point located at the center of the funnel, which was highly electronegative.⁵⁰ In **1** the same kind of saddle point is observed, but whereas the potential in the chromium wheel decreases from around zero outside the host to a minimum of $-1.24 \text{ e}/\text{\AA}$, the potential in **1** goes from $0.051 \text{ e}/\text{\AA}$ near the hydrogen bonded hexagon of the host structure to $0.014 \text{ e}/\text{\AA}$ at the center of the cavity, and hence, the electrostatic interaction energy with a potential guest molecule will be much weaker for **1**. The potential difference of the two cavities results in different affinity toward molecular groups. In the chromium wheel the electronegative cavity attracts the electropositive groups of the molecular guests, and hence, the electronegative group is expected to point out of the cavity. This indeed was observed to be the case for a number of chromium wheel host–guest complexes, and thus, the electrostatic potential of the interior of the host chromium wheel could be used to explain the orientation of the guest molecules. In **1** the center of the cavity is almost electro-neutral, but moving along the cavity in the direction of the *c*-axis the potential increases, which suggests that molecules situated in the cavity should have the electronegative region pointing in these directions. On the other hand, positively charged atoms of the molecule should be located in the center of the cavity as

suggested by Zubkus et al.¹⁵ However, in **1** the guest molecule cannot point out of the cavity, and the question arises how asymmetric molecules with electropositive and electronegative ends such as acetonitrile or methanol would behave in the cavity of the structure. Such molecules will not have a preferential orientation in the cavity, as either direction will result in unfavorable interactions in the symmetric cavity. The structural models reported in literature show that the acetonitrile molecules are ordered in the cavity of β -HQ (at room temperature), whereas the methanol molecules are disordered. In the ordered system, the asymmetric molecule will most likely be perturbed by the electric field in the cavity, as it cannot obtain electrostatic complementarity at both ends. This means that inclusion of such guest molecules presumably alters the charge distribution both of the host and the guest entities. The encapsulation of molecules in the clathrate is not merely an optimization of electrostatic forces, but a result of more complex molecular interactions. Host–guest interactions are normally to a first approximation considered as electrostatic interactions, but the present results suggest that archetypical host–guest systems, such as **1**, actually are governed by more complex interactions, and this may make predictions based on simple electrostatic arguments less precise.

CONCLUSION

The experimental CD of the metastable structure of **1** was determined using multipole modeling of synchrotron X-ray diffraction data obtained from a microcrystal at 15 K. Hirshfeld surface analysis of the intermolecular close contacts reveals directional C–H \cdots π interactions between the two interconnecting hydrogen bonded frameworks, and the nonhydrogen bond interactions account for more than 69% of the Hirshfeld surface. The weaker and more subtle intermolecular interactions

are clearly visible in the fingerprint plots, and this highlights the applicability of the Hirshfeld surface approach. The experimental multipole density exhibits single peak deformation densities in the bonds as well as negative oxygen core regions. Both these features signify that the experimental electron density is of high quality. The theoretical and experimental charge densities show good agreement, and charges obtained from Hirshfeld partitioning are similar although small distinct differences are present. In general, the hydrogen atoms are more positive in the theoretical model, whereas the oxygen atom is more negative. The electrostatic interaction energy, which is contributing the most to the total interaction energy, was determined from the theoretical and experimental models and they are comparable in magnitude, but with the theoretical value being substantially higher. As a result of these differences, the electrostatic potentials of the two models have small differences. Thus, the electronegative region of the hydroxyl oxygen atom is more dominant in the theoretical model. Investigation of the cavity of the empty host lattice showed that the electrostatic potential is very shallow and highly symmetric. Asymmetric molecules with an electropositive and an electronegative end would have no clear preferential orientation, as either direction will result in unfavorable interactions in the symmetric cavity, and the inclusion presumably is not merely a result of electrostatic optimization.

ASSOCIATED CONTENT

S Supporting Information. PXRD data of the as-synthesized and aged (14 days) material, differences of mean-squares displacement amplitudes, selected residual density maps, and residual density distribution plots. This material is available free of charge via the Internet at <http://pubs.acs.org>.

AUTHOR INFORMATION

Corresponding Author

*E-mail: bo@chem.au.dk.

ACKNOWLEDGMENT

This work was supported by the Australian Research Council, the Danish National Research Foundation (Center for Materials Crystallography), the Danish Strategic Research Council (Center for Energy Materials), and the Danish Research Council for Nature and Universe (DanScatt). ChemMatCARS Sector 15 is principally supported by the National Science Foundation/Department of Energy under Grant Number NSF/CHE-0822838. Use of the Advanced Photon Source was supported by the U.S. Department of Energy, Office of Science, Office of Basic Energy Sciences, under Contract No. DE-AC02-06CH11357.

REFERENCES

- (1) Desiraju, G. R. *Nature* **2001**, *412*, 397.
- (2) Reinbold, J.; Buhlmann, K.; Cammann, K.; Wierig, A.; Wimmer, C.; Weber, E. *Sens. Actuators, B* **1994**, *18*, 77.
- (3) Soldatov, D. V.; Enright, G. D.; Zanina, A. S.; Sokolov, I. E. *J. Supramol. Chem.* **2002**, *2*, 441.
- (4) Desiraju, G. R. In *Comprehensive Supramolecular Chemistry*; Vol. 6, Solid State Supramolecular Chemistry: Crystal Engineering, MacNicol, D. D., Toda, F., Bishop, R., Eds.; Pergamon: Oxford, 1996; p 1.
- (5) Spackman, M. A.; Byrom, P. G. *Chem. Phys. Lett.* **1997**, *267*, 215.
- (6) Spackman, M. A.; McKinnon, J. J. *J. CrystEngComm.* **2002**, *378*.
- (7) Turner, M. J.; McKinnon, J. J.; Jayatilaka, D.; Spackman, M. A. *CrystEngComm.* **2011**, *13*, 1804.
- (8) Powell, H. M. *J. Chem. Soc.* **1948**, *61*.
- (9) Palin, D. E.; Powell, H. M. *J. Chem. Soc.* **1948**, *815*.
- (10) Palin, D. E.; Powell, H. M. *J. Chem. Soc.* **1948**, *571*.
- (11) Mak, T. C. W. *J. Chem. Soc., Perkin Trans. 2* **1982**, *1435*.
- (12) Lindeman, S. V.; Shklover, V. E.; Struchkov, Y. T. *Acta Crystallogr., C: Cryst. Struct. Comm.* **1981**, *10*, 1173.
- (13) Mak, T. C. W.; Lam, C. K. *Encycl. Supramol. Chem.* **2004**, *679*.
- (14) Caspari, W. A. *J. Chem. Soc.* **1927**, *1093*.
- (15) Zubkus, V. E.; Shamovsky, I. L.; Tornau, E. E. *J. Chem. Phys.* **1992**, *97*, 8617.
- (16) Clausen, H. F.; Chevallier, M. S.; Spackman, M. A.; Iversen, B. B. *New J. Chem.* **2010**, *34*, 193.
- (17) Wallwork, S. C.; Powell, H. M. *J. Chem. Soc., Perkin Trans. 2* **1980**, *641*.
- (18) SAINT+, SADABS, XPREP, SHELXS and SHELXTL programs included in the Bruker SMART CCD software (Vers. 7.34A), Bruker Advanced X-ray Solutions, Inc.: Madison, WI, 2004.
- (19) Wu, G.; Rodrigues, B. L.; Coppens, P. *J. Appl. Crystallogr.* **2002**, *35*, 356.
- (20) Sheldrick, G. M. SADABS, Bruker AXS area detector Scaling and Absorption Correction; University of Göttingen: Göttingen, 2008.
- (21) Blessing, R. H. *J. Appl. Crystallogr.* **1997**, *30*, 421.
- (22) Evans, D. F.; Richards, R. E. *J. Chem. Soc.* **1952**, *3932*.
- (23) Rayner-Canham, G. *Descriptive Inorganic Chemistry*, 2nd ed.; W. H. Freeman and Company: New York, 2000.
- (24) Gibson, A. A. V.; Goc, R.; Scott, T. A. *J. Magn. Reson.* **1976**, *24*, 103.
- (25) Volkov, A.; Macchi, P.; Farrugia, L. J.; Gatti, C.; Mallinson, P.; Richter, T.; Koritsanszky, T. XD2006 (a computer program for multipole refinement, topological analysis of charge densities and evaluation of intermolecular energies from experimental or theoretical structure factors); State University of New York at Buffalo: Buffalo, NY, 2006.
- (26) Dittrich, B.; Koritsanszky, T.; Luger, P. *Angew. Chem., Int. Ed.* **2004**, *43*, 2718.
- (27) Dittrich, B.; Koritsanszky, T.; Grosche, M.; Scherer, W.; Flaig, R.; Wagner, A.; Krane, H. G.; Kessler, H.; Riemer, C.; Schreurs, A. M. M.; Luger, P. *Acta Crystallogr., B* **2002**, *58*, 721.
- (28) Madsen, A. O. *J. Appl. Crystallogr.* **2006**, *39*, 757.
- (29) Hansen, N. K.; Coppens, P. *Acta Crystallogr., A* **1978**, *34*, 909.
- (30) Allen, F. H.; Kennard, O.; Watson, D. G.; Brammer, L.; Orpen, A. G.; Taylor, R. *J. Chem. Soc., Perkin Trans. 2* **1987**, *S1*.
- (31) Hirshfeld, F. L. *Acta Crystallogr., A* **1976**, *32*, 239.
- (32) Harel, M.; Hirshfeld, F. L. *Acta Crystallogr., B* **1975**, *31*, 162.
- (33) Overgaard, J.; Clausen, H. F.; Platts, J. A.; Iversen, B. B. *J. Am. Chem. Soc.* **2008**, *130*, 3834.
- (34) Meindl, K.; Henn, J. *Acta Crystallogr., A* **2008**, *64*, 404.
- (35) Rees, B. *Acta Crystallogr., A* **1976**, *32*, 483.
- (36) Frisch, M. J.; Trucks, G. W.; Schlegel, H. B.; Scuseria, G. E.; Robb, M. A.; Cheeseman, J. R.; Montgomery, J. A., Jr.; Vreven, T.; Kudin, K. N.; Burant, J. C.; Millam, J. M.; Iyengar, S. S.; Tomasi, J.; Barone, V.; Mennucci, B.; Cossi, M.; Scalmani, G.; Rega, N.; Petersson, G. A.; Nakatsuji, H.; Hada, M.; Ehara, M.; Toyota, K.; Fukuda, R.; Hasegawa, J.; Ishida, M.; Nakajima, T.; Honda, Y.; Kitao, O.; Nakai, H.; Klene, M.; Li, X.; Knox, J. E.; Hratchian, H. P.; Cross, J. B.; Bakken, V.; Adamo, C.; Jaramillo, J.; Gomperts, R.; Stratmann, R. E.; Yazyev, O.; Austin, A. J.; Cammi, R.; Pomelli, C.; Ochterski, J. W.; Ayala, P. Y.; Morokuma, K.; Voth, G. A.; Salvador, P.; Dannenberg, J. J.; Zakrzewski, V. G.; Dapprich, S.; Daniels, A. D.; Strain, M. C.; Farkas, O.; Malick, D. K.; Rabuck, A. D.; Raghavachari, K.; Foresman, J. B.; Ortiz, J. V.; Cui, Q.; Baboul, A. G.; Clifford, S.; Cioslowski, J.; Stefanov, B. B.; Liu, G.; Liashenko, A.; Piskorz, P.; Komaromi, I.; Martin, R. L.; Fox, D. J.; Keith, T.; Al-Laham, M. A.; Peng, C. Y.; Nanayakkara, A.; Challacombe, M.; Gill, P. M. W.; Johnson, B.; Chen, W.; Wong, M. W.; Gonzalez, C.; Pople, J. A. *Gaussian 03*, revision C.02; Gaussian, Inc.: Wallingford, CT, 2004.
- (37) Jayatilaka, D.; Grimwood, D. J. *Lect. Notes Comput. Sci.* **2003**, *2660*, 142.

- (38) Hirshfeld, F. L. *Theor. Chim. Acta* **1977**, *44*, 129.
- (39) Lebedev, V. I.; Skorokhodov, A. L. *Dokl. Akad. Nauk* **1992**, *324*, 519.
- (40) Mura, M. E.; Knowles, P. J. *J. Chem. Phys.* **1996**, *104*, 9848.
- (41) Wolff, S. K.; Grimwood, D. J.; McKinnon, J. J.; Jayatilaka, D.; Spackman, M. A. *Crystal Explorer*, V. 2.0.0 alpha (r367); University of Western Australia: Australia, 2005–2007.
- (42) Figgis, B. N.; Iversen, B. B.; Larsen, F. K.; Reynolds, P. A. *Acta Crystallogr., B* **1993**, *49*, 794.
- (43) Poulsen, R. D.; Jorgensen, M. R. V.; Overgaard, J.; Larsen, F. K.; Morgenroth, W. G.; Graber, T.; Chen, Y. S.; Iversen, B. B. *Chem.—Eur. J.* **2007**, *13*, 9775.
- (44) Bader, R. F. W. *Atoms in Molecules: A Quantum Theory*; Oxford University Press: New York, 1990.
- (45) Abramov, Y. A. *Acta Crystallogr., A* **1997**, *53*, 264.
- (46) Espinosa, E.; Molins, E.; Lecomte, C. *Chem. Phys. Lett.* **1998**, *285*, 170.
- (47) Belof, J. L.; Stern, A. C.; Eddaoudi, M.; Space, B. *J. Am. Chem. Soc.* **2007**, *129*, 15202.
- (48) Poulsen, R. D.; Bentien, A.; Chevalier, M.; Iversen, B. B. *J. Am. Chem. Soc.* **2005**, *127*, 9156.
- (49) Hübschle, C. B.; Dittrich, B. *J. Appl. Crystallogr.* **2011**, *44*, 238–240.
- (50) Overgaard, J.; Iversen, B. B.; Palii, S. P.; Timco, G. A.; Gerbeleu, N. V.; Larsen, F. K. *Chem.—Eur. J.* **2002**, *8*, 2775.